Journal name
000(00):1–13
©The Author(s) 2010
Reprints and permission:
sagepub.co.uk/journalsPermissions.nav
DOI:doi number
http://mms.sagepub.com

A bounded iterative closest point method for minimally invasive registration of the femur

F. Rodriguez y Baena* **and T. Hawke**
Department of Mechanical Engineering, Imperial College London, UK

M. Jakopec
Stanmore Implants Worldwide Ltd., UK

Abstract

This paper describes a novel method for image-based, minimally invasive registration of the femur, for application to computer-assisted unicompartmental knee arthroplasty (UKA). The method is adapted from the well-known iterative closest point (ICP) algorithm. By utilising an estimate of the hip centre on both the preoperative model and intraoperative patient anatomy, the proposed 'bounded' ICP algorithm robustly produces accurate varus-valgus and anterior-posterior femoral alignment with minimal distal access requirements. Similar to the original ICP implementation, the bounded ICP algorithm converges monotonically to the closest minimum, and the presented case includes a common method for global minimum identification. The bounded ICP method has shown to have exceptional resistance to noise during feature acquisition through simulations and *in vitro* plastic bone trials, where the its performance is compared to a standard form of the ICP algorithm.

Keywords
Intraoperative registration; Computer-assisted surgery; UKA; Image-based; Minimally invasive

1. Introduction

In many cases of isolated knee osteoarthritis, unicompartmental knee arthroplasty (UKA) is reported to be a preferable treatment to total knee arthroplasty (TKA), producing equal or superior postoperative joint functionality while preserving healthy ligaments, cartilage and bone stock (1; 2; 3). Because much of the knee structure is maintained, UKA has lent itself to the application of minimally invasive surgery (MIS), in which the entire implantation process is performed through a single, short incision without dislocating the patella or severing the quadriceps tendon. MIS methods for UKA have been claimed in independent studies to significantly reduce blood loss, healing time and scarring while remaining capable of producing satisfactory implant placement (4; 3; 5). Despite these advantages, however, minimally invasive UKA is a more technically demanding procedure than conventional open surgery. The smaller incision drastically reduces the area

* Corresponding author; email: f.rodriguez@imperial.ac.uk

of accessible bone surface, as well as the surgeon's visibility. Figure 1 shows the typical accessible surface of the distal femur during minimally invasive medial UKA. Owing to the reduced access and visibility, risks of longer surgery time and improper implant placement are increased.

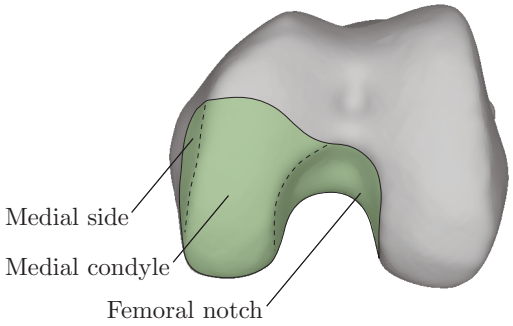

Fig. 1. Areas of the distal femur surface accessible during minimally invasive medial UKA.

It is widely suggested that improper placement of the implant components can lead to uneven wear and, in some cases, joint loosening, making revision surgery necessary (6; 7). Varus-valgus (coronal) rotation is the most commonly cited variable used to determine the success of prosthesis placement, as it primarily affects the alignment of the postoperative mechanical axis.

In recent years, computer assisted surgery (CAS) systems have been utilised in minimally invasive UKA in order to mitigate human error and the surgeon's lack of visibility and access. Some of these systems are now commercially available (e.g. *Curve*™, Brainlab AG, *OrthoMap ASM Knee Navigation*, Stryker), while others are still under development (e.g. (8)). Among these, the use of a 'hands-on' robotic manipulator for bone cutting has been shown to increase the accuracy of prosthesis placement compared with the manual approach (9). Clearly, there are a large number of factors contributing to the accurate placement of implant components in computer assisted UKA. Among the most influential of these is intraoperative registration: the acquisition of an accurate mapping between the space of the patient anatomy in the operating room (OR) and the space of the surgical plan. Errors accrued during this stage of the procedure will directly affect the alignment of the implanted prosthesis and are often difficult to detect intraoperatively, owing to the lack of a gold standard to assess registration accuracy 'on the fly'.

CAS systems in orthopaedics fall into two main categories, depending on the planning and registration methods involved: image-free and image-based systems. In image-free CAS systems, plans are generated intraoperatively on the back of surface and kinematic measurements of the limb, with (e.g. (10), (11)) or without (e.g. (12)) the aid of a statistical shape model. Such systems are gaining traction among the surgical community owing to the reduced preoperative planning time requirements for the surgeon and absence of ionizing radiation for the patient. The accuracy and robustness of these systems, however, may deteriorate if access to the bone surface is restricted (13; 14). Consequently, in computer assisted UKA, registration is often carried out using image-based methods (15; 13).

In image-based schemes, a coordinate measuring device is used to acquire features, often in the form of point clouds, either from identifiable objects such as fiducial marker screws or directly from the accessible bone surface. These features are then fitted to a preoperative computed tomography (CT) model of the anatomy, typically using some variant of the iterative closest point (ICP) algorithm (16; 17; 15). Such methods can produce accurate registration under normal operating conditions, although the outcome is highly reliant on a good fit between intraoperative surface measurements and the preoperative model. With the reduced access of a minimally invasive UKA procedure, registration outcome can quickly degenerate, as the acquisition of meaningful surface features is impaired. The result is an ambiguous match between the surfaces to be co-registered and, ultimately, an unacceptable surgical outcome.

Efforts continue to be made in developing completely non-invasive registration techniques, allowing accurate localisation using entire bone surfaces without the need for physical access. These methods generally make use of intraoperative medical images acquired from a known-position scanning device. Two imaging techniques have been well documented in the context of orthopaedic surgery: ultrasound imaging and fluoroscopy.

Many methods for ultrasound registration are similar in principle to the point-touching method, with the coordinate measuring device replaced by a hand-held ultrasound scanner (18; 19). Percutaneous images of the bone surface are acquired and processed, along with preoperative image data, to calculate the position and orientation of the bone relative to the scanner. During image acquisition, the scanner is tracked within the OR (with an optical tracking system, for example) producing a complete mapping between the CT model and the patient anatomy.

Fluoroscopic methods can either be used to track fiducial markers (20) or bone anatomy directly (21), and typically use a fixed position or tracked C-arm fluoroscope. While images can be much cleaner than those produced by ultrasound imaging, the use of X-rays does present the drawback of increasing the patient's radiation exposure.

Despite efforts to optimise acquisition and processing, for example by eliminating model reconstruction (22), intraoperative image-based registration methods are still inherently slower than digitisation methods. Extra calibration steps are often required to ensure proper image formation, and significantly more time is spent in data acquisition due to the necessary image segmentation. Furthermore, the large volume of data gathered increases computational load during convergence. In addition to increased surgery time, image-based methods naturally require the presence of an imaging device in the OR, introducing substantial financial costs and an increased intraoperative footprint.

In an attempt to improve the robustness of minimally invasive UKA registration without an increase in hardware complexity, this paper proposes a 'bounded' ICP method, which can be seen as an extension of the surface-based ICP algorithm used for anatomical registration (15) (from here, the 'standard ICP algorithm'). In this application, the method makes use of the functional hip centre to optimise the alignment of the femoral mechanical axis in terms of varus-valgus and anterior-posterior angular components. Contrary to the method described by Maurer et al. (23; 24), the bounded ICP algorithm does not make use of weighted contributions to register the hip centre and distal surface points simultaneously. Rather, the intraoperatively estimated hip centre is fixed in two translational degrees of freedom to that of the preoperative model, and thus only surface-based registration of the distal points is necessary. Aligning the mechanical axis of the femur in this way mitigates errors incurred during distal point collection, such that few points collected via the minimally invasive surgical site incision for UKA can reliably produce an accurate registration transform.

The bounded ICP method has previously been mentioned in the literature (25), however this paper fully describes the mathematical formulation and implementation of the associated algorithm.

Section 2 of this paper provides an overview of the theory and implementation of the proposed algorithm, while its experimental validation is described and discussed in sections 3 and section 4, respectively. Finally, conclusions are drawn in section 5.

2. Bounded ICP registration method

2.1. Theory

The following descriptions make use of anatomical notation based on the mechanical axis of the femur, as shown in figure 2. The mechanical axis is defined to pass through the centres of rotation of the hip and the knee.

The bounded ICP method makes use of a specifically selected remote point to constrain convergence of the standard ICP algorithm, effectively reducing the registration problem from six degrees of freedom to four. In doing so, accurate alignment of a given axis may be achieved. In the case presented, features on the distal femur are digitised through the same incision used to access the surgical site. An intraoperative navigation system records the position of the points, which approximate the knee centre of rotation. The functional centre of rotation of the hip is used to constrain the convergence of

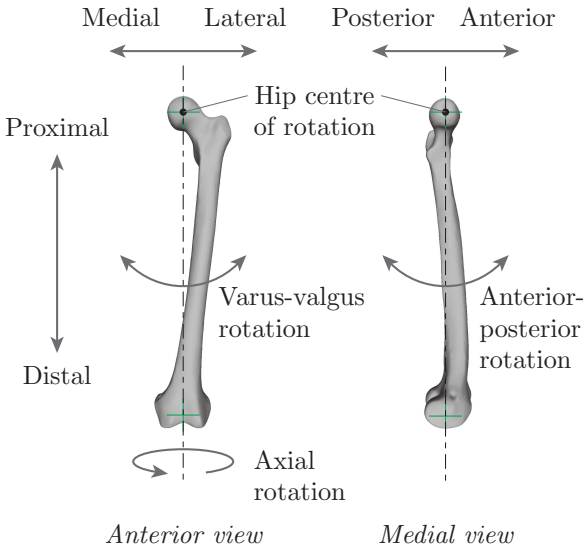

Fig. 2. Anatomical notation for orientation of the femur mechanical axis.

these points to a preoperative, three-dimensional (3D) CT model, guaranteeing varus-valgus/anterior-posterior registration errors within bounds dependent on the accuracy of the hip centre estimate.

In order to constrain the convergence of the ICP algorithm, the selected remote point must be acquired both intraoperatively and from the preoperative model. Previous studies have included methods for reliably locating the functional centre of rotation of the hip *in vivo* (26; 27) and from 3D CT model data(28). These methods involve no specialised apparatus other than that already used in any computer-assisted UKA procedure.

An illustration of the bounded convergence scheme is shown in figure 3. Angle α and the direction of the axis about which it is measured (ε) represent the varus-valgus/anterior-posterior degrees of freedom of the distal point-set. β represents axial rotation and δ indicates that the point-set may translate axially away from or towards the model hip centre.

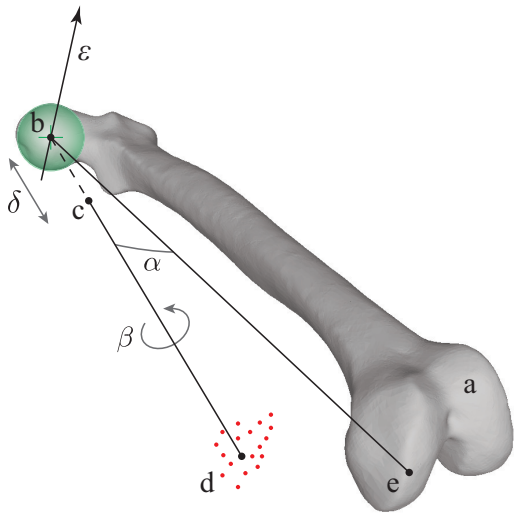

Fig. 3. Illustrative model of the convergence process. Here, a is the preoperative CT scan model, b is the hip centre estimated from CT model, c is the hip centre estimated intraoperatively, d is the distal point-set gathered intraoperatively and e is the centroid of corresponding points on the CT model surface. α represents the varus-valgus/anterior-posterior rotational degrees of freedom about axis ε, β represents the axial rotational degree of freedom and δ represents the axial translation.

Because the distance between the hip centre and the distal point-set is large compared to that between any two distal points, errors incurred during distal point acquisition have a reduced effect on the mechanical axis alignment compared to the standard ICP method. Indeed, assuming a $400\,\mathrm{mm}$ average femur length and correct distal registration, a medial-lateral or anterior-posterior translational error of $10\,\mathrm{mm}$ in the hip centre estimate will lead to only $\sim 1.4^\circ$ of varus-valgus or anterior-posterior registration misalignment.

2.2. Algorithm

The purpose of the registration procedure is to find the transformation between two arbitrary frames of reference such that features defined in one frame can be expressed in the other. In the case of computer-assisted UKA, the rigid transform $\mathbf{T}$ (rotation and translation) maps $\{R\}$, the robot reference frame, onto $\{M\}$, the CT model reference frame, such that, for an arbitrary position vector $\mathbf{p}$:

$$\mathbf{p}_{\{M\}} = \mathbf{T}\mathbf{p}_{\{R\}} \tag{1}$$

As the algorithm presented is iterative, the *current estimate* of $\mathbf{T}$ is denoted by $\mathbf{T}_n$, where n is the iteration number. In general, a subscript n represents a quantity in $\{M\}$ during iteration n.

Prior to registration, the necessary prerequisite data are gathered. Preoperatively, the hip centre $\mathbf{h}_M$ is acquired from the 3D CT model in $\{M\}$ by assuming it to be the centre of a sphere fitted to the femoral head surface. In the OR, the hip centre $\mathbf{h}_P$ is acquired using the functional method described in (26). N_P points $\mathbf{p}_i$ are collected directly from the available surface of the distal femur using a digitising probe. $\mathbf{h}_P$ and $\mathbf{p}_i$ are recorded in $\{R\}$.

As with the standard ICP algorithm, a reasonable initial transform estimate $\mathbf{T}_0$ is required to ensure accurate convergence. This is obtained by applying a least squares minimisation algorithm (29) to a set of corresponding point pairs, collected from known landmarks on the exposed femur and the CT model. Once all $\{R\}$ quantities have been transformed into $\{M\}$ by $\mathbf{T}_0$, the point-set is translated to make the hip centres $\mathbf{h}_M$ and $\mathbf{h}_{P0}$ coincident. This ensures that the centre of rotation is bound to the hip centre for the remainder of the algorithm.

Each iteration of the convergence process occurs in two stages, producing an improved transform estimate $\mathbf{T}_{n+1}$. Stage I minimises the varus-valgus/anterior-posterior angle between the approximated mechanical axes, as well as accounting for hip centre and distal point acquisition errors by allowing axial translation. Stage II optimises the axial alignment of the distal point-set and the CT model about the approximated mechanical axis.

Stage I The 'measured' mechanical axis – that belonging to the femur in the OR – is approximated as the axis that passes through both $\mathbf{h}_P$ and $\mathbf{k}_P$, where $\mathbf{k}_P$ is the centroid of the distal points in frame $\{R\}$:

$$\mathbf{k}_P = \frac{1}{N_P}\sum_{i=1}^{N_P}\mathbf{p}_i \tag{2}$$

In the ICP algorithm, corresponding points between the two modalities are defined to be those closest to one another by Euclidean distance. This implementation uses an optimised k-d tree search to calculate closest points, as detailed in (30). The points corresponding to $\mathbf{p}_{i,n}$ are denoted for each iteration by $\mathbf{c}_{i,n}$.

The 'model' mechanical axis passes through $\mathbf{h}_M$ and $\mathbf{k}_{Cn}$, where $\mathbf{k}_{Cn}$ is the centroid of the corresponding points $\mathbf{c}_{i,n}$:

$$\mathbf{k}_{Cn} = \frac{1}{N_P}\sum_{i=1}^{N_P}\mathbf{c}_{i,n} \tag{3}$$

The mean translational error $\mathbf{e}_n$ between the collected distal points and their corresponding model points is given by:

$$\mathbf{e}_n = \mathbf{k}_{Cn} - \mathbf{k}_{Pn} \tag{4}$$

To minimise this error while constraining about the hip centre, a translation of all points by $\mathbf{e}_n$ (see section 2.4) is approximated by a rotation θ_n about axis $\mathbf{a}_n$ and a translation $\mathbf{t}_n$ as shown in figure 4a. In mathematical form, let:

$$\mathbf{s}_n = \mathbf{k}_{Pn} - \mathbf{h}_M \tag{5}$$

and

$$\mathbf{q}_n = \mathbf{s}_n + \mathbf{e}_n \tag{6}$$

Axis $\mathbf{a}_n$ is defined by:

$$\mathbf{a}_n = \mathbf{s}_n \times \mathbf{q}_n \tag{7}$$

The angle of rotation θ_n is given by:

$$\theta_n = \cos^{-1}\left(\frac{\mathbf{s}_n \cdot \mathbf{q}_n}{\|\mathbf{s}_n\| \cdot \|\mathbf{q}_n\|}\right) \tag{8}$$

Note that because $\mathbf{a}_n$ is normal to the mechanical axis, θ_n has only varus-valgus and anterior-posterior components.

The translation along $\mathbf{q}_n$ is calculated by:

$$\mathbf{t}_n = (\|\mathbf{q}_n\| - \|\mathbf{s}_n\|) \cdot \frac{\mathbf{q}_n}{\|\mathbf{q}_n\|} \tag{9}$$

Phase I thus results in transformation $\mathbf{R}_1$:

$$\mathbf{R}_1 = R(\mathbf{a}_n, \theta_n) + T(\mathbf{t}_n) \tag{10}$$

The approximation $\mathbf{R}_1 \approx T(\mathbf{e}_n)$ is valid provided that the distance between the hip centre and the distal point-set is large compared with the distance between any two distal points:

$$\begin{aligned} &\forall i \in [1, N_P], \|\mathbf{k}_P - \mathbf{h}_P\| \gg \|\mathbf{k}_P - \mathbf{p}_i\| \\ &\implies \mathbf{R}_1 \approx T(\mathbf{e}_n) \end{aligned} \tag{11}$$

The product of stage I is the transform $\mathbf{T}'_n$, which applies $\mathbf{R}_1$ to $\mathbf{T}_n$.

$$\mathbf{T}'_n = T(\mathbf{h}_M)\, \mathbf{R}_1\, T(-\mathbf{h}_M)\, \mathbf{T}_n \tag{12}$$

Stage II Stage II minimises the mean angular error Φ_n between measured points and corresponding points about the axis $\mathbf{s}'_n$, where:

$$\mathbf{s}'_n = \mathbf{k}'_{Pn} - \mathbf{h}_M \tag{13}$$

and

$$\mathbf{k}'_{Pn} = \mathbf{T}'_n \mathbf{k}_P \tag{14}$$

In order to find the angular displacement error of each point $\phi_{i,n}$, we first define:

$$\mathbf{u}_{i,n} = \mathbf{p}_{i,n} - \mathbf{h}_M \tag{15}$$

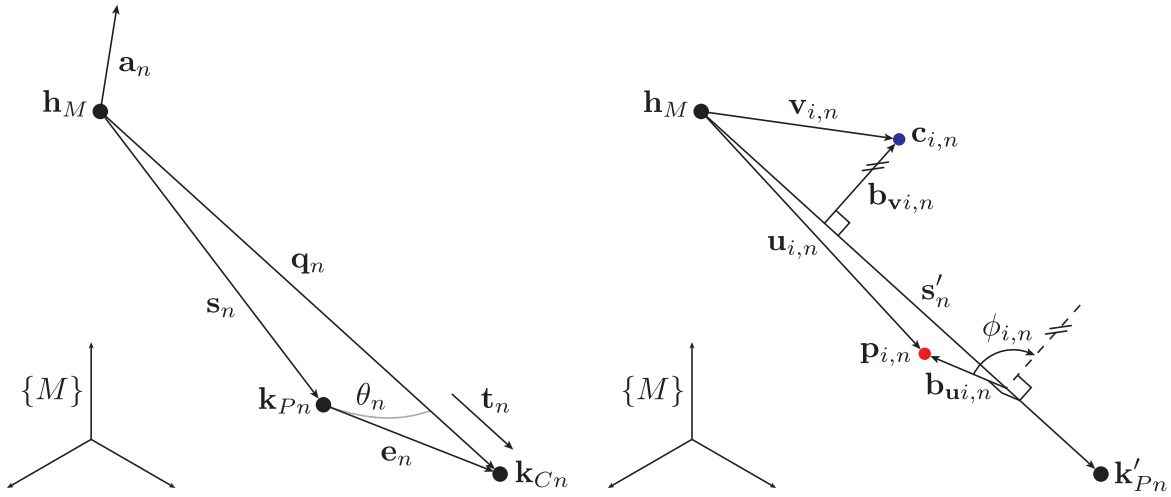

(a) Phase I. (b) Phase II.

Fig. 4. Phases of the bounded ICP convergence process. Position vectors are omitted for clarity.

$$\mathbf{v}_{i,n} = \mathbf{c}_{i,n} - \mathbf{h}_M \tag{16}$$

The components of $\mathbf{u}_{i,n}$ and $\mathbf{v}_{i,n}$ perpendicular to $\mathbf{s}'_n$ are given by:

$$\mathbf{b}_{\mathbf{u}i,n} = \mathbf{u}_{i,n} - \left(\frac{\mathbf{u}_{i,n} \cdot \mathbf{s}'_n}{\|\mathbf{s}'_n\|} \frac{\mathbf{s}'_n}{\|\mathbf{s}'_n\|} \right) \tag{17}$$

$$\mathbf{b}_{\mathbf{v}i,n} = \mathbf{v}_{i,n} - \left(\frac{\mathbf{v}_{i,n} \cdot \mathbf{s}'_n}{\|\mathbf{s}'_n\|} \frac{\mathbf{s}'_n}{\|\mathbf{s}'_n\|} \right) \tag{18}$$

As shown in figure 4b, $\phi_{i,n}$ is defined as the angular displacement from $\mathbf{p}_{i,n}$ to $\mathbf{c}_{i,n}$ about $\mathbf{s}'_n$:

$$\begin{aligned} \phi_{i,n} = & \operatorname{sgn}\left((\mathbf{b}_{\mathbf{u}i,n} \times \mathbf{b}_{\mathbf{v}i,n}) \cdot \mathbf{s}'_n \right) \\ & \cdot \cos^{-1}\left(\frac{\mathbf{b}_{\mathbf{u}i,n} \cdot \mathbf{b}_{\mathbf{v}i,n}}{\|\mathbf{b}_{\mathbf{u}i,n}\| \|\mathbf{b}_{\mathbf{v}i,n}\|} \right) \end{aligned} \tag{19}$$

Finally:

$$\Phi_n = \frac{1}{N_P} \sum_{i=1}^{N_P} \phi_{i,n} \tag{20}$$

The result of stage II is the rotation transform $\mathbf{R}_2$, which, when applied to $\mathbf{T}'_n$, results in $\mathbf{T}_{n+1}$:

$$\mathbf{R}_2 = R(\mathbf{s}'_n, \Phi_n) \tag{21}$$

$$\mathbf{T}_{n+1} = T(\mathbf{h}_M)\, \mathbf{R}_2\, T(-\mathbf{h}_M)\, \mathbf{T}'_n \tag{22}$$

In order to monitor the convergence of the algorithm, the root mean squared (RMS) error between collected points and their corresponding counterparts on the 3D model is calculated after each iteration. In the current implementation, the algorithm runs until the difference between RMS errors from successive iterations falls below a specified threshold, or once a specified number of iterations has been reached. The latter case often suggests that registration was not successful.

2.3. Suppression of local minima

The 3D surface-based registration problem is non-convex and, as such, minimising error to a global minimum can be difficult (31). In this implementation, perturbations are applied to solutions produced by the bounded ICP algorithm in order to ensure the global minimum is reached (32). The local minimum suppression mechanism has two steps.

First, the correct 'class' of minima (i.e. that containing the global minimum) must be identified. In order to achieve this, the bounded ICP algorithm is repeatedly run using only stage I. Once convergence has been achieved, a rotational perturbation of the point-set of a random angle about a random axis perpendicular to the mechanical axis and passing through the model hip centre is executed.

The correct class of local minima is identified by inspecting the magnitude of the RMS error following convergence. In testing, distant local minima have consistently produced substantially higher RMS values compared to local minima nearby the global minimum.

In the second step, the algorithm is allowed to converge fully, with both stage I and stage II. After each run, the current registration estimate is perturbed by a random angle about the mechanical axis. The process is repeated a set number of times. The global minimum is identified by the registration transform that produces the lowest RMS error.

2.4. Convergence

During every iteration of the bounded ICP algorithm, the mean translational error $\mathbf{e}_n$ is minimised, also minimising the mean-squared (MS) error (and thus the RMS error) of the acquired point-set. This means that the same convergence theorem described in (16, *B. Convergence Theorem*, p. 244) can be used to prove that this algorithm will converge monotonically to the closest local minimum.

3. Experimental validation

The performance of the bounded ICP algorithm has been systematically evaluated by means of simulation and plastic bone trials, with meaningful comparisons drawn against the standard ICP algorithm. Details and results of these tests are provided below. Benchmark acceptable registration component errors of $2\,^\circ$ rotation and $2\,\mathrm{mm}$ translation (based on estimated surgical accuracy as per (33)) are used to gauge the success of the registration outcomes. All experiments consider a medial UKA procedure, thus the surgically accessible bone surface is defined according to figure 1, although a virtually identical approach can be applied to the remaining two compartments.

3.1. Simulation

For the purposes of developing and testing the bounded ICP algorithm, a versatile simulator was implemented in C++ and OpenGL. The simulator graphically displays the progress of the registration convergence on-screen, as well as allowing manual step-through functionality if desired. Random or selectively distributed point-sets can be rapidly generated and processed, such that the bounded ICP method (or any other implemented registration algorithm) can be tested for a wide range of input data. The simulated environment also crucially provides the ability to measure absolute registration accuracy – a quantity which is unobtainable in the OR.

One thousand point-sets were randomly generated from a single 3D distal femur model using the surface region accessible during minimally invasive UKA. A population of 100 point-sets was generated to represent each point-set size N_P for $N_P \in \{10, 15, 20, 25, 30, 35, 40, 50, 75, 100\}$. In each population, random noise was added to point-sets evenly grouped into 5 levels of maximum noise magnitude ranging between $0\,\mathrm{mm}$ and $2\,\mathrm{mm}$. For testing the bounded ICP algorithm, a hip centre estimate was generated for each point-set, with a constant 'worst-case' estimate (28) of $10\,\mathrm{mm}$

error from the actual centre. These errors were applied in random directions. The initial transform estimate was simulated by perturbing the generated point-set from the model by $5\,^{\circ}$ and $5\,\mathrm{mm}$ in random directions.

For each point-set, both the standard and the bounded ICP algorithm were run, and the resulting absolute registration error matrices were recorded.

3.2. Plastic bone trials

Laboratory tests with a phantom femur and pelvis were carried out to corroborate the findings of the simulation platform. CT scans of a plastic left femur (Sawbones Ltd., ITEM# 1100) were taken and segmented into a 3D model before the femoral head was restrained into the acetabulum of the pelvis using elastic restraints. The pelvis was clamped rigidly to an operating table. Figure 5 shows the experimental setup.

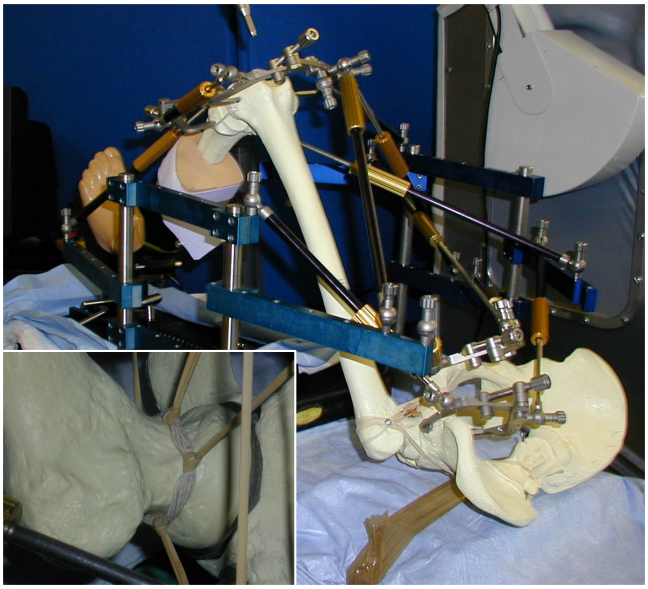

Fig. 5. Acquisition of the distal femur points in plastic bone trials with a commercial robotic system for UKA (Stanmore Implants Worldwide Ltd.). Inset: femoral head held in position by elastic restraints.

A ground truth registration transform was calculated by fixing the femur in position and using the standard ICP algorithm to fit points collected from the entire femur surface to the CT model. Ten consecutive full registration procedures were carried out using both the standard and the bounded ICP algorithms. For each trial, a new point set with an average of 20 points was acquired and used as the input for both registration methods. For the bounded method, the hip centre was estimated for each registration using the functional method described in (26) with an average of 400 points. All points on the femur were acquired using a commercially available robotic system for UKA (Stanmore Implants Worldwide Ltd.). Absolute error components of the registration matrices produced (varus-valgus rotation, anterior-posterior rotation, axial rotation and overall translation) were calculated by comparison with the ground truth transform.

Further tests were carried out to investigate the correlation between hip estimation error and overall registration error in the bounded method. For the 10 registrations described, the *actual* hip centre was calculated by transforming the modelled hip centre (from the CT data) by the ground truth registration. The error in the 10 hip centre estimates was then evaluated and, using basic trigonometry, predicted error components of the registrations were calculated.

4. Results and discussion

4.1. Simulation

Figure 6 shows the results of the simulation tests in terms of femur alignment components and overall translational error.

Registration outcome, in terms of varus-valgus and anterior-posterior alignment differs considerably between the two chart sets. Regardless of the point-set size and maximum noise value, both the varus-valgus and anterior-posterior charts can be approximated to a plane for the bounded ICP algorithm in figure 6b. More specifically, the two planes indicate approximately $0.5\,^{\circ}$ rotational error, which is in accordance with the average result for a maximum hip centre error of $10\,\mathrm{mm}$.

The translation and axial rotation components of the registration error matrices show similar characteristics for both the standard and bounded ICP algorithm. Both of these alignments deteriorate as a function of the quality of the distal point-set, indicating that a small number of inaccurate points is not sufficient to accurately describe the femoral geometry for axial alignment. A comparison of the axial rotation errors for both algorithms provides some evidence for a weakness in the bounded ICP algorithm. Since the movement of one end of the femoral mechanical axis is restricted, noise in the distal point-set results in a large number of minima with near identical RMS error values, but different axial rotation-translation pairs. Although these minima lie within an envelope bounded by the extent of the noise, this characteristic of the bounded ICP algorithm produces a less even chart for axial rotational error compared to that of the standard algorithm.

Despite this characteristic, a set of 25 distal points is sufficient to consistently produce a registration transform error within $2\,^{\circ}$ and $2\,\mathrm{mm}$ for axial rotation and translation respectively, assuming a worst case of $2\,\mathrm{mm}$ maximum acquisition error.

4.2. Plastic bone trials

Table 1 shows the calculated registration error components for the standard and bounded ICP algorithms across the 10 trials. The values shown were used to compare the algorithms by means of four one-tailed F-tests for variance equality – one for each error component. For both varus-valgus and anterior-posterior rotation, the variances of the bounded ICP errors were found to be significantly lower than those of the standard ICP algorithm at the 5% level ($p = 0.0001$ and $p = 0.0014$, respectively). This corroborates the findings from the simulation and suggests that the bounded ICP algorithm can more reliably produce accurate axial alignment between the preoperative and intraoperative data. As expected, no statistically significant difference was found for the axial rotation or translational errors ($p = 0.1295$ and $p = 0.0936$, respectively).

The results show that the bounded ICP algorithm can repeatedly produce registration transforms well within $2\,^{\circ}$ rotation and $2\,\mathrm{mm}$ translation in a minimally invasive UKA setting. As well as the varus-valgus and anterior-posterior rotation errors being significantly lower than the benchmark values, the translational errors recorded are also noticeably low (mean $0.29\,\mathrm{mm}$, standard deviation $0.11\,\mathrm{mm}$). This suggests that the algorithm reliably rejects local minima distant from the global minimum during convergence.

Both simulated and phantom trials also highlight how the accuracy of the intraoperative hip centre estimate can be readily correlated to the overall registration outcome. As predicted, it was found that certain hip estimate error components proportionally affect particular registration error components, with varus-valgus alignment bound to medial-lateral hip error and anterior-posterior alignment bound to anterior-posterior hip error. Also as predicted, the proximal-distal hip centre estimate was found not to affect the registration outcome, as the bounded ICP algorithm allows translation along the mechanical axis. These results demonstrate the bounded ICP algorithm's ability to shift the requirements for an accurate varus-valgus/anterior-posterior registration away from the quality of the distal point-set.

Table 2 shows estimated varus-valgus and anterior-posterior rotation error components derived from the given hip centre estimate errors. The prediction errors – the differences between the predicted and actual registration error components of the bounded method – are also shown. These values indicate that varus-valgus and anterior-posterior registration error

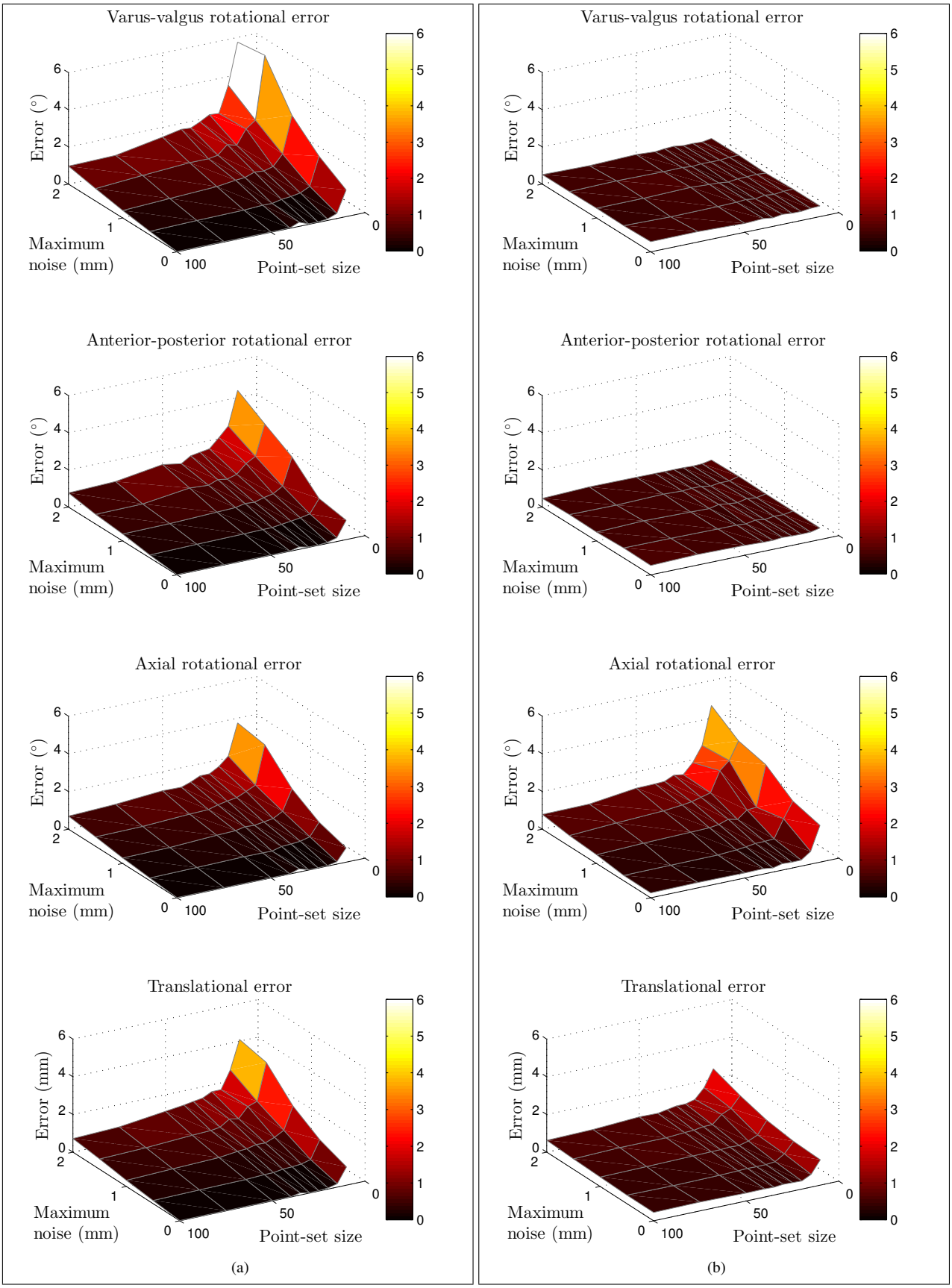

Fig. 6. Simulation registration accuracy results – shown as the mean of the absolute registration error components – for a) the standard ICP implementation and b) the bounded ICP algorithm.

		Registration test number									
		1	2	3	4	5	6	7	8	9	10
Registration error components (Standard ICP)											
V-V	(°)	-0.18	1.06	0.33	1.02	0.24	0.07	0.29	-0.60	1.02	0.37
A-P	(°)	-0.44	-1.00	-0.51	-1.56	-0.35	0.38	-0.85	0.29	-0.63	-0.17
Axial	(°)	-0.60	1.35	1.18	2.00	1.09	0.18	0.88	0.10	0.67	0.64
Trans	(mm)	0.58	0.13	0.37	0.57	0.53	0.43	0.32	0.18	0.34	0.16
Registration error components (Bounded ICP)											
V-V	(°)	0.14	0.21	0.22	0.27	0.38	0.42	0.18	0.09	0.21	0.01
A-P	(°)	-0.53	-0.66	-0.80	-0.70	-0.95	-0.74	-1.08	-1.11	-0.76	-1.00
Axial	(°)	1.81	0.75	0.99	0.61	0.72	0.84	0.66	0.36	-0.06	0.31
Trans	(mm)	0.24	0.16	0.38	0.34	0.49	0.33	0.35	0.20	0.31	0.16

Table 1: Registration error components for 10 consecutive procedures computed with both the standard and bounded ICP algorithms on a plastic bone. Error matrices are calculated relative to the ground truth transform. *V-V*: Varus-valgus rotation, *A-P*: Anterior-posterior rotation/translation, *Axial*: Axial rotation, *Trans*: Overall translation.

		Registration test number									
		1	2	3	4	5	6	7	8	9	10
Hip centre error components											
M-L	(mm)	-1.17	-1.65	-1.39	-2.20	-2.70	-3.26	-1.15	-0.44	-1.52	0.49
A-P	(mm)	-3.18	-4.97	-6.13	-5.40	-7.56	-5.58	-8.13	-8.64	-5.79	-8.12
P-D	(mm)	8.12	0.01	0.23	2.76	0.69	5.63	-6.14	-8.60	0.36	-9.66
Estimated registration error components											
V-V	(°)	0.15	0.21	0.18	0.28	0.35	0.42	0.15	0.06	0.19	0.06
A-P	(°)	-0.40	-0.64	-0.79	-0.69	-0.97	-0.72	-1.04	-1.11	-0.74	-1.04
Prediction error											
V-V	(°)	0.01	0.00	-0.04	0.01	-0.03	0.00	-0.03	-0.03	-0.02	0.05
A-P	(°)	0.13	0.02	0.01	0.01	-0.02	0.02	0.04	-0.00	0.02	-0.04

Table 2: Predicted registration error components for the bounded ICP trials, based on known hip centre errors. *M-L*: Medial-lateral translation, *A-P*: Anterior-posterior rotation/translation, *P-D*: Proximal-distal translation, *V-V*: Varus-valgus rotation.

components can be consistently estimated to well within $0.2\,\mathrm{mm}$ if the error of the hip estimate is known, and that the registration outcome for the bounded ICP method is directly proportional to the quality of the hip centre estimate.

5. Conclusion

The bounded ICP method has shown to be a robust means for femoral registration, and produces reliable and repeatable results with realistic minimally invasive UKA data. Phantom bone experiments using existing intraoperative hardware indicate that the bounded ICP algorithm is capable of reliably registering a physical femur against a preoperative CT model to well within $2\,^\circ$ and $2\,\mathrm{mm}$ of error, assuming the overall point touching accuracy to be within $2\,\mathrm{mm}$. *In vitro* comparison of the bounded method with the standard ICP algorithm (typically used for this type of procedure) highlights a statistically significant improvement in terms of varus-valgus/anterior-posterior mechanical axis alignment. In all trials, the algorithm has been found to reject final convergence to a local minimum. The clear correlation between the registration outcome and the hip centre estimate indicates that, by ensuring that the hip centre estimation procedure produces a reliable result, it is possible to bound the outcome of the femoral registration process.

Contrary to non-invasive registration methods, which overcome the limitations of reduced surgical access by including intraoperative imaging systems, the bounded ICP algorithm runs at very low computational expense. Additionally, no hardware is required that is not already available during minimally invasive UKA, nor does the process need any bone access other than that presented by the arthroplasty procedure.

The bounded ICP method is particularly suited to registration of long bones such as the femur, where an estimable point is present on the axis to be aligned, and suitably distant from the acquired point-set. For instance, registration of the tibia may be achieved using a proximal point set and an estimate of the ankle centre derived from digitisation of the malleoli through the skin.

Due to the constraints on bone features, the bounded ICP method is not directly applicable to a large number of orthopaedic registration scenarios with all of the advantages of the application described. However, provided that the necessary data are available pre- and intraoperatively, the algorithm may be adapted to provide optimal alignment between any two modalities along a desired axis.

In the current study, it has been assumed that features acquired intraoperatively do not suffer from systematic bias, for instance that which would be caused by the presence of image artefacts in the patient model which do not appear on the exposed surface of the bone. Future work will thus focus on extensions of this method to improve the registration's susceptibility to non-Gaussian noise in the sensed features.

References

[1] Cartier P, Sanouiller JL, Grelsamer RP. Unicompartmental knee arthroplasty surgery. The Journal of Arthroplasty. 1996 Oct;11(7):782–8.

[2] Newman JH, Ackroyd CE, Shah NA. Unicompartmental or total knee replacement? The Journal of Bone and Joint Surgery. 1998 Sep;80(5):862–865.

[3] Yang KY, Wang MC, Yeo SJ, Lo NN. Minimally invasive unicondylar versus total condylar knee arthroplasty–early results of a matched-pair comparison. Singapore Medical Journal. 2003 Nov;44(11):559–62.

[4] Price AJ, Webb J, Topf H, Dodd CAF, Goodfellow JW, Murray DW. Rapid recovery after Oxford unicompartmental arthroplasty through a short incision. The Journal of Arthroplasty. 2001 Dec;16(8):970–976.

[5] Müller PE, Pellengahr C, Witt M, Kircher J, Refior HJ, Jansson V. Influence of minimally invasive surgery on implant positioning and the functional outcome for medial unicompartmental knee arthroplasty. The Journal of Arthroplasty. 2004 Apr;19(3):296–301.

[6] Barrett WP, Scott RD. Revision of failed unicondylar unicompartmental knee arthroplasty. The Journal of Bone and Joint Surgery American Volume. 1987 Dec;69(9):1328–35.

[7] Hernigou P, Deschamps G. Alignment Influences Wear in the Knee after Medial Unicompartmental Arthroplasty. Clinical Orthopaedics and Related Research. 2004 Jun;423:161–165.

[8] Hungr N, Roger B, Hodgson AJ, Plaskos C. Dynamic Physical Constraints: Emulating Hard Surfaces with High Realism. IEEE Transactions on Haptics. 2012 Jan;5(1):48–57.

[9] Rodriguez F, Harris S, Jakopec M, Barrett A, Gomes P, Henckel J, et al. Robotic clinical trials of uni-condylar arthroplasty. The International Journal of Medical Robotics and Computer Assisted Surgery. 2005 Dec;1(4):20–8.

[10] Rajamani KT, Joshi SC, Styner MA. Bone model morphing for enhanced surgical visualization. In: IEEE International Symposium on Biomedical Imaging: Nano to Macro, 2004. vol. 2; 2004. p. 1255–1258.

[11] Barratt DC, Chan CSK, Edwards PJ, Penney GP, Slomczykowski M, Carter TJ, et al. Instantiation and registration of statistical shape models of the femur and pelvis using 3D ultrasound imaging. Medical Image Analysis. 2008 Jun;12(3):358–74.

[12] Jenny JY, Boeri C. Unicompartmental knee prosthesis implantation with a non-image-based navigation system: rationale, technique, case-control comparative study with a conventional instrumented implantation. Knee Surgery, Sports Traumatology, Arthroscopy: Official Journal of the ESSKA. 2003 Jan;11:40–45.

[13] Pearle AD, O'Loughlin PF, Kendoff DO. Robot-assisted unicompartmental knee arthroplasty. The Journal of Arthroplasty. 2010 Feb;25(2):230–7.

[14] Audenaert E, Smet B, Pattyn C, Khanduja V. Imageless versus image-based registration in navigated arthroscopy of the hip: a cadaver-based assessment. The Journal of Bone and Joint Surgery British Volume. 2012 May;94(5):624–9.

[15] Jakopec M, Harris SJ, Rodriguez y Baena F, Gomes P, Cobb J, Davies BL. The first clinical application of a “hands-on" robotic knee surgery system. Computer Aided Surgery. 2001 Jan;6(6):329–39.

[16] Besl PJ, McKay ND. A Method of Registration of 3-D Shapes. IEEE Transactions on Pattern Analysis and Machine Intelligence. 1992;14(2):239–56.

[17] La Palombara PF, Fadda M, Martelli S, Marcacci M. Minimally invasive 3D data registration in computer and robot assisted total knee arthroplasty. Medical & Biological Engineering & Computing. 1997 Nov;35(6):600–10.

[18] Amin DV, Kanade T, DiGioia AM, Jaramaz B. Ultrasound registration of the bone surface for surgical navigation. Computer Aided Surgery. 2003 Jan;8:1–16.

[19] Barratt DC, Penney GP, Chan CSK, Slomczykowski M, Carter TJ, Edwards PJ, et al. Self-calibrating 3D-ultrasound-based bone registration for minimally invasive orthopedic surgery. IEEE Transactions on Medical Imaging. 2006 Mar;25(3):312–323.

[20] Otake Y, Armand M, Armiger RS, Kutzer MD, Basafa E, Kazanzides P, et al. Intraoperative Image-based Multiview 2D/3D Registration for Image-Guided Orthopaedic Surgery: Incorporation of Fiducial-Based C-Arm Tracking and GPU-Acceleration. IEEE Transactions on Medical Imaging. 2012;31(4):948–962.

[21] Livyatan H, Yaniv Z, Joskowicz L. Gradient-Based 2-D/3-D Rigid Registration of Fluoroscopic X-Ray to CT. IEEE Transactions on Medical Imaging. 2003;22(11):1395–1406.

[22] Brooks R, Collins DL, Morandi X, Arbel T. Deformable ultrasound registration without reconstruction. In: Metaxas DN, Axel L, Fichtinger G, Szekely G, editors. Medical Image Computing and Computer-Assisted Intervention: MICCAI 2008. New York City, USA: Springer-Verlag Berlin Heidelberg; 2008. p. 1023–31.

[23] Maurer CR, Aboutanos GB, Dawant BM, Maciunas RJ, Fitzpatrick JM. Registration of 3-D images using weighted geometrical features. IEEE Transactions on Medical Imaging. 1996 Jan;15(6):836–49.

[24] Maurer CR, Maciunas RJ, Fitzpatrick JM. Registration of head CT images to physical space using a weighted combination of points and surfaces. IEEE Transactions on Medical Imaging. 1998 Oct;17(5):753–761.

[25] Rodriguez y Baena F, Davies B. Robotic surgery: from autonomous systems to intelligent tools. Robotica. 2009 Aug;28(02):163.

[26] Leardini A, Cappozzo A, Catani F, Toksvig-Larsen S, Petitto A, Sforza V, et al. Validation of a functional method for the estimation of hip joint centre location. Journal of Biomechanics. 1999 Jan;32(1):99–103.

[27] Siston RA, Delp SL. Evaluation of a new algorithm to determine the hip joint center. Journal of Biomechanics. 2006 Jan;39(1):125–30.

[28] Rodriguez y Baena F. Improving Accuracy in Robotic Assisted Orthopaedic Surgery. Imperial College London; 2004.

[29] Horn BKP. Closed-form solution of absolute orientation using unit quaternions. Journal of the Optical Society of America A, Optics and Image Science. 1987;4(4):629–42.

[30] Friedman JH, Bentley JL, Finkel RA. An Algorithm for Finding Best Matches in Logarithmic Expected Time. ACM Transactions on Mathematical Software. 1977;3(3):209–26.

[31] Ma B, Ellis RE. Robust registration for computer-integrated orthopedic surgery: laboratory validation and clinical experience. Medical Image Analysis. 2003 Sep;7(3):237–250.

[32] Cuchet E, Knoplioch J, Dormont D, Marsault C. Registration in neurosurgery and neuroradiotherapy applications. Journal of Image Guided Surgery. 1995 Jan;1(4):198–207.

[33] Cobb J, Henckel J, Gomes P, Harris S, Jakopec M, Rodriguez F, et al. Hands-on robotic unicompartmental knee replacement: a prospective, randomised controlled study of the acrobot system. The Journal of Bone and Joint Surgery British Volume. 2006 Feb;88(2):188–197.